Numerical Evaluation of The Nonlinear Behavior of Soil-Pile Interaction Under The Effect of Coupled Static-Dynamic Loads

Duaa Al-Jeznawi
UiTM: Universiti Teknologi MARA
ISMACAHYADI Mohamed Jais (ismac821@uitm.edu.my)
UiTM: Universiti Teknologi MARA
Bushra S. Albusoda
University of Baghdad

Research Article

Keywords: Numerical analyses, liquefaction, coupled static-dynamic load, acceleration, far-field, and soil-pile interaction

Posted Date: December 30th, 2021

DOI: https://doi.org/10.21203/rs.3.rs-1201856/v1

Abstract

Liquefaction of saturated soil layers is one of the most common causes of structural failure during earthquakes. Liquefaction occurs as a result of increasing pore water pressure, whereby the rise in water pressure occurs due to unexpected change in stress state under short-term loading, i.e., shaking during an earthquake. Thus, general failure occurs when the soil softens and eliminates its stiffness against the uplift pressure from the stability of the subsurface structure. In this case, the condition of soil strata is considered undrained because there is not enough time for the excess pore water pressure to dissipate when a sudden load is applied. To represent the non-linear characteristics of saturated sand under seismic motions in Kobe and Ali Algharbi earthquakes, the computational model was simulated using the UBCSAND model. The current study was carried out by adopting three-dimensional-based finite element models that were evaluated by shaking table tests of a single pile model erected in the saturated soil layers. The experimental data were utilized to estimate the liquefaction and seismicity of soil deposits. According to the results obtained from the physical models and simulations, this proposed model accurately simulates the liquefaction phenomenon and soil-pile response. However, there are some differences between the experiment and the computational analyses. Nonetheless, the results showed good agreement with the general trend in terms of deformation, acceleration, and liquefaction ratio. Moreover, the displacement of liquefied soil around the pile was captured by the directions of vectors generated by numerical analysis, which resembled a worldwide circular flow pattern. The results revealed that during the dynamic excitation, increased pore water pressure and subsequent liquefaction caused a significant reduction in pile frictional resistance. Despite this, positive frictional resistance was noticed through the loose sand layer (near the ground surface) until the soil softened completely. It is worth mentioning that the pile exhibited excessive settlement which may attribute to the considerable reduction, in the end, bearing forces which in turn mobilizing extra end resistance.

1 Introduction

Several studies have recently focused on the effect of dynamic excitation on the soil-structure behavior. The phenomena of soil fluidization have been noticed and considered a major concern when the soil layers are fully saturated. Terzaghi and Peck in 1967, presented a new phenomenon named "spontaneous liquefaction" and they described it as an abrupt loss of a soil strength of the loose sand, which in turn created flow slides owing to a minor disturbance. Mogami and Kubo (1953) reported the same occurrence noted after earthquakes. This phenomenon has been studied extensively since 1964 due to the Niigata earthquake which was definitely the incident that brought the soil liquefaction to the attention globally. In 1964 and 1995, two larger earthquakes in Niigata and Kope, respectively, demonstrated the magnitude and scope of destruction that soil liquefaction may produce (Robertson and Wride 1998). Therefore, liquefaction was considered as a significant design flaw for constructions in saturated sand soils i.e., earth dams. Mory et al. (2007), studied the effect of the intense wave loading on a vertical wall and the liquefaction was significantly detected at the wall toe. Sakai et al. in 1992, identified the liquefaction phenomenon in the sand as a transient phenomenon, and Michallet et al. in 2009 stated that this phenomenon was caused by the trapped air bubbles inside the soil layers. Tzang and Ou in 2006, named this phenomenon as soil fluidization and stated that the critical over-pressure (for liquefaction development) is reached when the excess pore water pressure becomes close to the static soil pressure. In fact, the excess pore water pressure develops inside the soil as a result of the cyclic loading of an earthquake. This increase in pore pressure may cause a significant reduction in soil strength, thus in turn the soil layer behaves as a liquid-like form. Kenan H. and Maksat O. in 2019, studied seismic excitation of an actual soil layer, they used 29 saturated sand samples and performed a set of laboratory experiments to investigate the seismic loadings. Their results showed

that the liquefaction phenomenon is less pronounced at the soil layer in shallow depth. Additionally, even if the produced excess pore pressure is not high enough to induce liquefaction collapse, yet the pressure dissipation produces huge damage due to excessive settlement. Consequently, a failure of saturated sand soils may be attributed to the liquefaction phenomenon and/or excessive settlement. Many researchers (Suzuki H., et al. 2008; Tokimatsu K., et al. 2007; and Tamura S. with Tokimatsu K., 2006) investigated the soil-structure interaction in saturated soil layers via shaking table tests. Tokimatsu K. et al. in 2004, conducted shaking table tests with large-scale models in dry and saturated soils to study the piles under the kinematic and inertial effect of earthquakes. The findings showed that these forces have influenced the pile stresses if the natural period of the pile exceeds that of the ground.

The above literature showed that a shaking table test might come up with a realistic comprehension of the soil-structure interaction under earthquake excitation. Furthermore, this test is taking less time and is low-cost as compared with full-scale tests of foundation (Altaee and Fellenius 1994). However, because of the different scaling low, developing advanced physical models are not straightforward. According to Altaee and Fellenius (1994), the difference between the results of the 1g physical model and the prototype may be attributed to the nonlinearity of a stress-strain behavior and the initial confining pressure. Despite the apparent benefits of shaking table tests, due to scale, the measured response may differ from the large-scale prototype response.

Ongoing researches in numerical modeling are capable of capturing the nonlinear behavior of three-dimensional models of the soil-pile system in varied ground situations (Hussein A. and El Naggar M. 2021). Numerical analysis may be able to take control of some of the drawbacks of the laboratory models, i.e., scaling (Cheng Z. and Jeremi ´c B. 2009), allowing for the validation of the experiment outputs and intense comprehension of various soil-pile system attributes. Several studies explored the attitude of piles in saturated sand soil using the latest advances in numerical analyses, such as realistic numerical models for soil manner and trustworthy time-domain solvers (Wang R. et al. 2016; Hussein A.F. and El Naggar M.H. 2021; and Elgamal A. and Lu J. 2009).

2 Evaluation Of The Effect Of Stress-strain Reversal During Soil Liquefaction

The majority of studies on the factors that cause saturated sands to liquefy have focused on the horizontal ground, in which a soil particle is supposed to be subjected to entirely reversed cycles of shear forces during an earthquake (Seed and Lee 1966; and Finn et al. 1971). Yoshiaki and Hrnosm in 1975 proposed the term "R" which describes the level of stress reversal and is described as the ratio of one direction's maximum shear stress to the other direction's maximum shear stress (Figure 1). The authors presented the magnitude of stress reversal in terms of the initial shear stress τ_0 and the dynamic shear stress τ_d:

$$R = (\tau_d - \tau_0)/ (\tau_d + \tau_0) \quad .....(1)$$

Robertson and Wride in 1998, stated that if the initial void ratio of a soil layer is greater than the ultimate state line (USL, this term is defined by Poorooshasb and Consoli 1991), the soil may experience strain softening (SS) under significant stresses, after a period of time reaching an optimum state known as a critical or steady-state.

The frequency of an earthquake excitation, which typically ranges from 0 to 15 Hz, reveals that loading cycles are a significant parameter affecting the liquefaction attitude of the soil layer (Silva, W.J. 1988). The influence of loading cycles on liquefaction of granular soils has been studied for a variable frequency ranging from 0.05 to 12

Hz, largely using cyclic triaxial experiments on saturated sand, and failure principles rely on the normal strain and the ratio of excess pore pressure. However, there are conflicts to the findings on the impact of loading frequency on soil liquefaction resistance. Many researchers have reported that the undrained cyclic strength of liquefiable soil may be insignificantly weak and unaffected by the frequency (Yoshimi, Y. and Oh-oka 1975; Wong, R.T. et al. 1975; Tatsuoka, F. et al. 1983; Tatsuoka, F. 1986; Polito, C.P. 1999; Wang, X.H. and Zhou, H.L. S. 2003; and Sze, H.Y. 2010). Yoshiaki and Hrnosm in 1975 stated that the degree of stress reversal had a significant impact on the initial liquefaction circumstances, but had no effect on the entire liquefaction conditions. Zhenzhen Nong et al. (2020) had concluded the previous studies related to the influence of loading cycles on the liquefaction phenomenon of granular soils, as shown in Table 1.

Table 1
Previous studies on loading cycles influence (Zhenzhen Nong et al. 2020).

No.	Ref.	Method of testing	Confining pressure (kPa)	Relative density %	Failure criteria	Number of cycles to liquefaction	Loading frequency (Hz)	Influence of loading
1	Yshimi and Oh-oka 1975	Cyclic torsional shear	33	37	r_u=1	Not available	1-12	none
2	Tatsuoka et al. 1983	Cyclic triaxial	98	50-80	ϵ_a = 10% double amplitude	10	0.05,0.5	
3	Polito 1999	Cyclic triaxial	100	74	r_u = 1	10, 15	0.5, 1	
4	Wong et al. 1975	Cyclic triaxial	100	60	r_u = 1	Not available	0,067, 0.33	Insignificant
5	Sze 2010	Cyclic triaxial	100- 500	10- 70	ϵ_a = 5% double amplitude	10	0.01, 1	
6	Peacock and Seed 1968	Simple shear	500	50	r_u = 1	10	0.17-4	Very small
7	Tatsuoka et al. 1986	Cyclic triaxial	100	50	ϵ_a = 10% double amplitude	10	0.05,1	
8	Wang and Zhou 2003	Cyclic triaxial	150	58	ϵ_a = 10% double amplitude	Not available	1,3,5	
9	Lee and Fitton 1969	Cyclic triaxial	100	50,75	ϵ_a = 5, 10, 20% double amplitude	30	0.17,1	Higher strength at higher frequency
10	Feng and Zhang 2013	Cyclic triaxial	100	30	ϵ_a = 5% double amplitude	20,30	0.05-2	
11	Zhang et al. 2015	Cyclic triaxial	100-300	25	r_u = 1	Not available	0.5-2	
12	Guo and He 2009	Cyclic triaxial	100-300	28,70	r_u = 1	12,30	0.05,0.1,1	
13	Mulilis et al. 1975	Cyclic triaxial	100	50	ϵ_a = 5% double amplitude	10	0.017,1	Higher strength at lower frequency

The effect of subsurface soil layers on ground shaking propagation is commonly quantified using earthquake site surveys (Oscar M. et al. 2018). Studies have suggested pore water pressure generating models to enhance the expected post-earthquake response such as; Vucetic 1986; Matasovic 1993; Seed et al. 1975; Martin et al. 1975;

Dobry et al. 1982 and 1985; Green et al. 2000; Green 2001; Polito et al. 2008; and Ivsic 2004) and soil models based on effective pressure (Wang et al. 2001; Elgamal et al. 2002; Park and Byrne 2004; Jefferies and Been 2006; and Boulanger and Ziotopoulou 2015) that may be employed for a field response of seismic analysis. Booker et al. 1976, was the first to present an effective stress-based model called “GADFLEA” to explore the development and dissipation of excess pore water pressure.

This study is developed to present how the dynamic excitation affects this attitude of sandy soils by developing the 3D numerical modeling via MIDAS GTS NX software and the results were validated with 1g shaking table findings.

3 Modified Ubcsand Model

UBCSAND is a plasticity constitutive model of effective stress that can be applied in advanced geotechnical stress deformation investigations and estimating the liquefaction phenomenon of sand under seismic excitation. The model was created particularly for sand-like soils that could liquefy under seismic stress (e.g., sands and silty sands with a relative density of less than roughly 80%). The model shows the soil's shear stress-strain behavior through the use of an implicit hyperbolic analysis. Michael and Peter in 2011, proposed that when drainage is constrained, fluid in the voids of sand serves as a volumetric restraint inside the soil. This limitation produces a rise in pore pressure, which can cause liquefaction. Chou et al., 2021 investigated the difference between the UBCSAND and Finn model and found that the UBCSAND model could capture the accumulation of the shear strain during dynamic excitation. Through using an implicit technique, the MIDAS GTS NX liquefaction model was adapted to a full 3D representation of the modified UBCSAND theory. The main difference between the implicit and the explicit techniques, whereby the latter predicts the behavior of the system at a later stage from the existing stage of the system, whereas implicit techniques establish a result by calculating an equation incorporating both the existing and the later stages of the system. The elastic modulus fluctuates depending on the effective stress exerted in the elastic zone, allowing nonlinear elastic attitudes to be modeled. Three forms of yield characteristics govern the response in the plastic zone: shear (shear hardening), compression (cap hardening), and pressure cut-off. The influence of soil densification can be considered by dynamic loading in the situation of shear hardening (MIDAS GTS NX, user manual).

The pore pressure ratio is calculated depending on the following equation:

$$Max.\ \frac{\Delta P_w}{P'_{init}}$$

… 2

Where: (ΔP_w) is the difference in excessive pore water pressure, $\left(P'_{init}\right)$ is the initial effective pressure.

4 Summary Of The Material Models And The Scaling Law

Figure 2 demonstrates the soil layers, pipe pile body, pile cap, ground surface spring, free field elements, interface elements, applied vertical and lateral static loads, and shows the corresponding finite element sizes.

The mass of the pile model in the numerical analysis was adjusted to have overall unit weight (30 kN/m^3) as in the laboratory tests. The interface parameters between the soil layers and pile were calculated depending on the

reduction factor ‘R’, which in turn is taken as 0.6 and 0.7 for elements between the pile and loose sand and the pile with dense sand, respectively as recommended by Ghalibafian 2006. In order to capture the precise soil-pile response, the model main parameters were calibrated, as presented in Table 2 and 3. Subsequently, the earthquake duration was scaled by multiplying the original acceleration time to ($\lambda^{0.75}$), and then the intended acceleration values were incorporated with the new time set.

Even though the reduced mesh size increases the analytical precision, the calculation time increase as well. However, because the current models need very fine mesh to capture the behavior of soil-pile interaction under different ground accelerations, tetrahedral elements of 0.04 m length were considered. Elements were distributed as the more zone density at the highly deformed area closed to the pile body, as shown in figure 3. A 4-node tetrahedral element was used to represent the soil layers, each element has four degrees of freedom: three for displacements and one for pore water pressure. The pile body and the pile cap were also discretized in a similar way with the soil elements. The problem was taken as an isotropic-elastic material for pile and pile cap, and isotropic-modified UBCSAND model for the loose and dense sand soil layers. In current numerical simulation, the laboratory model was scaled up ($\eta = 2$) by adapting Wood (2004) scaling law.

Table 2
Parameters for a modified UBCSAND model used in this study which is based on the calibration process presented in Beaty and Byrne 2011.

Parameter	Loose sand	Dense sand
Equivalent SPT blow count for clean sand $(N_1)_{60}$	15	30
Reference pressure (kPa)	101	101
Elastic shear modulus number (unitless)	1069	1347
Elastic shear modulus exponent (unitless)	0.5	0.5
Peak Friction Angle (°)	34.5	39
Constant Volume Friction Angle (°)	33	33
Cohesion (kPa)	1	1
Plastic shear modulus number (unitless)	821	3736
Plastic shear modulus exponent (unitless)	0.4	0.4
Failure ratio	0.73	0.66
Post Liquefaction Calibration Factor (Residual shear modulus)*	0.7	0.01
Soil Densification Calibration Factor (Cyclic Behavior)	0.45	0.45
Plastic/Pressure Cutoff (Tensile Strength kPa)	0	0
Saturated unite weight (kN/m^3)	19.5	21.5

**If the Max possible stress ratio is achieved, liquefaction is developed and the Plastic shear modulus number is decreased by Post Liquefaction Calibration Factor.*

Table 3
Pile and pile cap properties

Properties	Pile	Pile cap
Dimensions (m)	Do=0.032, Di=0.026	0.1 x 0.1 x 0.02
Unit weight (kN/m^3)	30	30
Modulus of elasticity (GPa)	67	67
Moment of inertia (m^4)	$4.36E^{-8}$	-
Cross-sectional area (m^2)	$2.7E^{-4}$	0.01
Damping ratio (ξ)	5%	5%

5 Boundary Conditions And Coupled Effective Stress Analysis Stages

For all sorts of analysis, MIDAS GTS NX offers a variety of boundary conditions. For static computations, this study used a 3-D element model and ground initial conditions. As illustrated in figure 4a, the bottom of the sandbox was set in the x-y-z directions, the front and back faces were fixed at the y-direction, and the right and left faces were fixed at the x-direction. For dynamic analysis, since the plane wave moves into the soil layers, the boundary condition should be maintained to eliminate wave reflection and to avoid the boundary influence. Since modeling infinite ground is beyond the bounds of possibility, two methods were employed in these models; one is applying plane free field elements at the soil box sides, and second, extruding the sides elements in a soil box for a long distance to obtain a wide model box which in turn assist in minimizing the wave reflections. However, the latter mothed was noticed as time-consuming, and no restriction rules are available, therefore, the free field elements were considered which are less time-consuming with correspond to more reasonable outputs.

The first stage in the model analysis was achieved by activating the static boundary conditions (figure 4a) to calculate the total stresses initiated by model self-weight. Then, adding a water table on the soil surface (create phreatic surface) to develop the problem of effecting coupled stresses on saturated soil below the groundwater table. Sequentially, the vertical static load and then the lateral static load were applied on a nonlinear soil constitutive model. Then, switching to the liquefiable layers by adopting the UBCSAND model and introducing the earthquake input motion. In the later stage, the static boundary was deactivated and switched by the elastic boundary conditions, as shown in figure 4b.

6 Soil-pile Deformation Due To Liquefaction

The soil deformation around the pile was explored to evaluate the compatibility between the numerical calculations and laboratory testing. To study the mechanism of liquefaction-induced significant soil-pile deformation, it is found that the two forms of modeling (using Kope and Ali Algharbi earthquakes) be consistent at the same time with the experiment results. Soil-pile deformation in the laboratory experiments (Hussein and Albusoda 2021) was presented by the vertical and horizontal displacements. Soil-pile deformation from the numerical modeling was further illustrated via MIDAS GTS NX. Figure 5 shows the contour lines and the vectors of the maximum total deformation of soil layers and figure 16 shows the maximum vertical and lateral deformation

of the pile, due to applying a couple of static loads (50% of the allowable vertical load and 50% of the allowable horizontal load) with two different ground acceleration (Kope and Ali Algharbi).

Dilatancy is a phenomenon related to dense soil subjected to shearing. In other word, when a dense sand layer experiences shear force, the overall volume of the intended layer increase. This phenomenon was observed by the current numerical model as shown in figure 5. The low liquefaction ratio in a dense sand layer may attribute to the dilation phenomenon which in turn considered as the liquefaction resistance (Madhira and Jaswant 2000). Thus, the phase transition was very noticeable in which the volumetric strain shifted from contraction in a loose sand layer to dilation in the dense sand layer.

From figure 5, it can be noticed from the direction of the vectors that the soil particles pushed aside during the dynamic excitation and the settlement of the soil increased as getting far from the pile body. Thus, the maximum soil settlement was observed at the far-field, similar observations were obtained by Chian and Madabhushi 2014 during the investigation of the uplift of the ground structures due to dynamic excitation.

Pile response during dynamic excitation is highly influenced by the nonlinearity of soil-pile interaction. The pile distortion during the high-intensity ground acceleration of Kope earthquake (around 0.82g) was clear in figure 6a, this deformation may be attributed to the material nonlinearity, cyclic loads during the high ground acceleration cause soil movement, which in turn affects the pile strength. As the loose soil softens due to liquefaction, the stresses around the pile start to diminish. In other words, as the soil loses its stiffness owing to liquefaction, the pile becomes an unstable column. Thus, the pile friction resistance will begin to deteriorate, and the pile may buckle as a result of existing an axial load on the pile cap. Manish et al. 2017, stated that the degree of pile deformation is controlled by pile's stiffness, depth of the saturated loose sand layer, and the intensity of the ground motion. As for the vertical settlement, it is likely that the pile will drop vertically or incline in one direction as a result of a complex effect of buckling and bending. In this manner instead of the pile is to resist both skin and end bearing resistance, the pile now is only resisting the end bearing, and this phenomenon will definitely reduce the geotechnical capacity to some extent because the contact surface area of the pile skin to resist the down drag effect has diminished (figure 16). This will not only cause buckling due to the loss of all-around stresses but will definitely cause a negative skin friction impact i.e. down drag to the pile if the end bearing is insufficient to cater for the geotechnical influence from the soil and also from the structural load.

On the other hand, the pile followed the soil motion during Ali Algharbi earthquake without a significant buckling or deformation as shown in figure 6b. That may be attributed to the low ground acceleration (around 0.1g), so the pile stiffness was enough to resist the ground shaking. In another word, the loss of skin friction of the pile is lower, due to lower vibration of the ground.

The above results were validated (by using the scaling law of Wood (2004)) by the experiment findings (Hussein and Albusoda 2021), as shown in figure 7. As predicted by numerical and experimental findings, the magnitude of the pile settlement increased with higher input acceleration (Kope earthquake). This indicates the considerable influence of shaking intensity on the soil-pile response as previously noted.

Based on these results, the pile displaced vertically and laterally relative to the surrounding soil during different load increments rather than a smooth 1-D movement as stated by Chian and Madabhushi 2012.

7 Near And Far-field Measurements Of Acceleration And Pore Water Pressure In Soil Layers

Excess pore-water pressure is expected to be developed in a liquefying soil layer, along with alleviation in seismic waves. The liquefaction ratio, R_u, is calculated by dividing the variation in pore pressure by the soil's initial effective vertical pressure. Figures 8 to 11 show the contour lines of the maximum state of how the water pressure ratio propagates through the soil layers of a different time. The results were in good agreement with the experiment findings (Hussein Albusoda 2021). Some other observations were also extracted from the MIDAS GTS NX outputs.

As presented in figures 8 and 9, the high-water pressure ratio at the far-field in the early stages (less than 10 seconds) may attribute to re-orientation of the soil particles away from the pile body during seismic excitation (as shown in figure 5a) which in turn trying to uplift the pile (as shown in figure 7a) giving high excess pore pressure at the far-field as compared to the elements near the pile at the same depth.

Based on the numerical analysis and experimental data, it appears that at all depths of the saturated sand sample, both the formation of excess pore pressure and the propagation of ground acceleration (Figures 11 and 13) from the model bottom to the surface soil were roughly similar.

The liquefaction phenomenon is generated roughly at a time of reaching the intense shaking (high ground acceleration) followed by pile drag down. Although this situation is not very clear under the effect of the Ali Algharbi earthquake due to low acceleration (around 0.1g), it is significantly noticed with the Kope earthquake (around 0.82g), figures 8, 9, 10, 11, and 12.

The current numerical models could capture the liquefaction propagation through the soil layers as shown in figures 10 and 12. In general, some differences were observed between the numerical outputs and the experimental findings may attribute for instance: to minor changes in the boundary condition that could cause such inconsistencies in the numerical modeling and the laboratory samples. On the other hand, the similarity in the general pattern of acceleration and liquefaction ratio time histories is noted, which is suitable for both modeling post-earthquake response and adequately calculating the movement of the pile embedded in the soil.

8 Undrained Behavior Of Sand Soil Under Coupled Of Static-dynamic Loads

Figure 14a and 15a show the shear stress-shear strain relationship of the soil element adjacent to the pile body at depth of 200 mm in the model. With the formation of extra pore-pressure, it is obvious that the shear strength of the soil (gained from interparticle frictional contact) is diminished. As a result of the build-up of high pore-water pressure (liquefaction initiation), it is supposed that the pile will settle. Based on figures 8 and 9, the loose soil layer softened after time 10 and 30 seconds under Kope and Ali Algharbi earthquakes, respectively, due to a significant increase in the excess pore pressure at that time. The sudden rise of pore water pressure attributes to the significant short-term undrained behavior of the soil at previously mentioned times since the soil model exhibit a significant dynamic wave increase (according to the input acceleration histories of Kope and Ali Algharbi earthquakes). Thus, the pile experienced a considerable downward movement, as shown in figure 7, due to loss of skin friction. This phenomenon was in an agreement with Mahmood S. (2009). The later stated that when soil liquefied, the mobilized shear stress tends to decrease, accompanied by large shear strain. The tendency becomes pronounced as the soil density decreases or the amount of injected pore water increases.

Chou et al. 2021 stated that a liquefaction constitutive model (UBCSAND) seeks to reproduce the crucial feature when the soil approaches the initial liquefaction point, which called banana loop during such shear force reversal, the plastic shear modulus decreases and increases (from positive values to negative ones and vice versa). Similar behavior was captured by MIDAS GTS NX, as shown in figures 14a and 15a.

It is noticed that the fictional resistance in dense sand is higher than of the loose one to some extent as shown in figure 16, which may be attributed to the shorter length of the shear zone in a loose sand layer and less effective weight of the surrounding soil in addition to the high liquefaction ratio which is recorded at shallow depths, as shown in figures 8 and 9. Overall, soil particles lose their shear strength and roughly behave as a slurry as noticed at the end of the laboratory tests, the numerical analyses could capture this behavior by decreasing the frictional resistance significantly during the dynamic excitation until it reaches the minimum value at the final stage.

9 Conclusion

The results of the proposed model of soil-pile interaction system were in good agreement with the 1g shaking table tests which were performed by Hussein and Albusoda 2021. The existing model accurately captured the soil-pile response under a coupled static-dynamic load. Providing a roughly similar trend and magnitude of soil layers and the embedded pile response under the effect of couple static (vertical and lateral loads) and dynamic loads, it is clear that numerical modeling via MIDAS GTS NX is able to produce a good representation of the soil-pile behavior in 1g shaking table test. It is observed that shear stresses for loose sand decreases during the dynamic excitation due to the propagation of excess pore water pressure, as noticed in figures 14b and 15b. In the dense sand deposit, there was some pore pressure buildup, but still not enough to produce liquefaction due to the densification of the dense sand. Smaller excess pore pressure in a dense sand layer indicates that some of the soil's shear strength has been preserved, which may provide some restriction to pile movement. In the strain-softening effect, the buildup of pore water pressure becomes negative i.e. dilation as the stress-strain response experiences peak and then ultimate stress. This is part of the element preserved through time history due to the compactness of the sand through time has caused significant sand particle densification which restricts partly the elevated pore water pressures due to small voids volume.

As seen in figures 10 and 12, this observation suggests that extra pore pressure was first initiated and developed in faraway from the pile body, resulting in stability of the pile during the 5 and 15 seconds of applying Kope and Ali Algharbi earthquakes respectively. Nonetheless, once the pile began to drop down, it was impeded by the frictional resistance of surrounding soil as it tried to re-orientate the particles away due to controlled dilation (figure 5). Pile buckling deformation was observed in numerical modeling during the application of high intense acceleration (Kope earthquake), as shown in figure 6a. It is suggested that to eliminate buckling, certain design considerations should be taken to enhance the pile's rigidity. The dimension of the pile can be increased based on the depth of the saturated loose sand and the boundary conditions at the top and bottom of the liquefied layer. Bending and buckling principles are interconnected and should not be considered separately since they will combine during an earthquake to induce pile failure.

The general trend and magnitude of pile displacement under the effect of the Kope earthquake was roughly closed to 1g shaking table and the current numerical model (figure 5a); However, the existing model slightly overestimated the vertical displacement of a pile under the effect of Ali Algharbi earthquake (figure 5b). This could address some the inconsistencies between the numerical model and the laboratory test, where these discrepancies may attribute to the general experimental setting-up, scaling law, boundary conditions, the accuracy of the strain gauge sensors,

and error tolerance of the analysis control setting-up of the existing numerical model. Despite the variations between the numerical model and 1g shaking test results, the overall response of the soil and pile were compared satisfactorily. Consequently, the existing model can be used to study different criteria or model properties that are not captured in physical modeling, as well as to overcome experimental modeling drawbacks such as restricted or difficult measurements or scaling effects. As a result, the present study uses verified numerical models to analyze the shear stress-strain relationship and frictional resistance, which were not addressed in the experimental program.

References

1. Terzaghi K, Peck RB (1967) Soil mechanics in engineering practice, 2nd edn. John Wiley & Sons, Inc., New York
2. Mogami T, Kubo K (1953) The behaviour of soil during vibration. In Proceedings of the 3rd International Conference on Soil Mechanics and Foundation Engineering, Vol. 1. pp. 152–153
3. Robertson PK, and Wride (née Fear) CE (1998) Cyclic liquefactionits evaluation based on the SPTCPT. In Proceedings of the 1996 NCEER Workshop on Evaluation of Liquefaction Resistance of Soils. Edited by T.L. YoudI.M. Idriss. NCEER-97-0022
4. Mory M, Michallet H, Bonjean D, Piedra-Cueva I, Barnoud J-M, Foray P, Abadie S, Breul P (2007) A field study of momentary liquefaction caused by waves around a coastal structure. ASCE J. Waterw. Port Coastal Ocean Eng. 133(1):28-38
5. Sakai T, Hatanaka K, Mase H (1992) Wave-induced effective stress in seabed and its momentary liquefaction. ASCE J Waterw Port Coast Ocean Eng 118(2):202–206
6. Hervé Michallet E, Catalano C, Berni B, Chareyre Valérie Rameliarison, Eric Barthélemy, ICSE6 Paris - August 27-31, 2013. https://hal.archives-ouvertes.fr/hal-00908807
7. Tzang SY, Ou SH (2006) Laboratory flume studies on monochromatic wave-fine sandy bed interactions. Part 1. Soil fluidization. Coastal Eng 53:965–982
8. Kenan Hazirbaba and Maksat Omarow (2019) Strain-based assessment of liquefaction and seismic settlement of saturated sand. Cogent Engineering 6:1573788
9. Suzuki H, Tokimatsu K, Sato M, Tabata K (2008) Soil-pile-structure interaction in liquefiable ground through multi-dimensional shaking table tests using E-Defense facility. Proc., 14th World Conference on Earthquake Engineering, Beijing, China
10. Tokimatsu K, Suzuki H, Tabata K, Sato M (2007) Three-dimensional shaking table tests on soil-pile-structure models using E-Defense facility. Proc., 4th international conference on earthquake engineering. June; 2007. p. 25–8
11. Tamura S, Tokimatsu K (2006) Seismic earth pressure acting on embedded footing based on large-scale shaking table tests. Seismic performance and simulation of pile foundations in liquefied and laterally spreading ground:83–96
12. Tokimatsu K, Suzuki H, Sato M (2004) Effects of inertial and kinematic forces on pile stresses in large shaking table tests. Proc., Proc., 13th World Conf. on Earthquake Engineering, Vancouver
13. Altaee A, Fellenius BH (1994) Physical modeling in sand. Can Geotech Journal 420:431–431

14. Hussein AH, El Naggar MH (2021) Effect of model scale on helical piles response established from shake table tests. Soil Dynamic and Earthquake Engineering 152 (2022) 107013
15. Cheng Z, Jeremi´c B (2009) Numerical modeling and simulation of pile in liquefiable soil. Soil Dynam Earthq Eng 29:1405–1416
16. Wang R, Fu P, Zhang JM (2016) Finite element model for piles in liquefiable ground. Comput Geotech 72:1–14
17. Elgamal A, Lu J (2009) A framework for 3D finite element analysis of lateral pile system response. In: Contemporary topics in in situ testing, analysis, and reliability of foundations; p. 616–23
18. Seed HB, Lee KL (1966) LIQUEFACTION OF SATURATED SANDS DURING CYCLIC LOADING. Journal of the Soil Mechanics and Foundations 92:105–134
19. Martin GR, Finn WL, Seed HB (1975) Fundementals of liquefaction under cyclic loading. J Geotech Geoenviron Eng 101:423–438
20. Yoshiaki Yoshimr and Hrnosm oh-oka (1975) Influence of degree of shear stress reversal on the liquefaction potential of saturated sand. Soils and foundations Vol. 15, No. 3, Japanese Society of Soil Mechanics and Foundation Engineering
21. Poorooshasb HB, Consoli NC (1991) The ultimate state. In Proceedings of the 9th Panamerican Conference on Soil Mechanics and Foundation Engineering, Vina del Mar, Chile, pp. 1083–1090
22. Silva WJ (1988) Soil Response to Earthquake Ground Motion (EPRI Report NP-5747); Electric Power Research Institute: Palo Alto, CA, USA
23. Wong RT, Seed HB, Chan CK (1975) Cyclic Loading Liquefaction of Gravelly Soils. J Geotech Geoenviron Eng 101:571–583
24. Tatsuoka F, Toki S, Miura S, Kato H, Okamoto M, Yamada S, Yasuda S, Tanizawa F (1986) Some Factors Affecting Cyclic Undrained Triaxial Strength of Sand. Soils Found 26:99–116
25. Polito CP (1999) The Effects of Non-plastic and Plastic Fines on the Liquefaction of Sandy Soils. Ph.D. Thesis, Virginia Polytechnic Institute and State University, Blacksburg, VA, USA
26. Wang XH, Zhou HL (2003) Study on dynamic steady state strength of sand soil liquefaction. J Rock Mech Eng 22:96–102
27. Sze HY, Thesis PhD (2010) Hong Kong University, Hong Kong, China
28. Zhenzhen Nong S-S, Park S-W, Jeong, Lee D-E (2020) Effect of Cyclic Loading Frequency on Liquefaction Prediction of Sand. Appl Sci 10:4502. doi:10.3390/app10134502
29. Tatsuoka F, Maeda S, Fujii S, Yamada SI (1983) Cyclic undrained strength of saturated sand under random and uniform loading and their relation. Bull. ERS (Institute of Industrial Science, Univ. of Tokyo), 16, 11–31
30. Mulilis JP, Seed HB, Chan CK, Mitchell JK, Arulanandan K (1977) Effects of sample preparation on sand liquefaction. Journal of the Geotechnical Engineering Division, ASCE 103(GT2):99–108
31. Chang-Nieto OMoreno-TorresG, Andrés, Salas-Montoya (2018) Evaluation of coupled porewater pressure and stress-strain constitutive model in granular soils. DYNA, vol. 85, no. 204, pp. 248-256, Universidad Nacional de Colombia
32. Vucetic M (1986) Pore pressure buildup and liquefaction at level sandy sites during earthquakes. Rensselaer Polytechnic Institute, Troy, NY
33. Matasovic N (1993) Seismic response of composite horizontally-layered soil deposits. University of California, Los Angeles, CA

34. Seed HB, Martin PP, Lysmer J (1975) The generation and dissipation of pore water pressure during soil liquefaction. Report No EERC-75-26. University of California, Berkeley, California, USA
35. Martin GR, Finn WDL, Seed HB (1975) Fundamentals of liquefaction under cyclic loading. J Geotech Engrg Div 101(5):423–438
36. Dobry R, Ladd RS, Yokel FY, Chung RM, Powell D (1982) Prediction of pore water pressure buildup and liquefaction of sands during earthquakes by the cyclic strain method., Building Science Series 183, National Bureau of Standards, U.S. Department of Commerce Washington D.C., USA
37. Green RA, Mitchell JK, Polito CP (2000) An energy-based excess pore pressure generation model for cohesionless soils, Proceedings of the John Booker Memorial Symposium, Sidney Australia, A.A Balkema Publishers, Rotterdam, Netherlands
38. Green RA (2001) Energy-based evaluation and remediation of liquefiable Soil. Virginia Polytechnic Institute and State University
39. Polito CP, Green RA, Lee J (2008) Pore pressure generation models for sands and silty soils subjected to cyclic loading., Journal of Geotechnical and Geoenvironmental Engineering, 134(10), pp. 1490-1500, 2008. DOI: 10.1061/(ASCE)1090- 0241(2008)134:10(1490), 1490-1500
40. Ivsic T (2006) A model for presentation of seismic pore water pressures, Soil Dynamic and Earthquake Engineering, 26, pp. 191-199, 2006. DOI: 10.1016/j.soildyn.2004.11.025
41. Wang ZL, Chang CY, Mok CM (2001) Evaluation of site response using downhole array data from a liquefied site, Proceedings: 4th International Conference on Recent Advances in Geotechnical Earthquake Engineering and Soil Dynamics and Symposium in Honor of Professor W.D. Liamn Finn, San Diego, California, USA
42. Yang Z, Elgamal A (2002) Influence of permeability on liquefaction-induced shear deformation., Journal of Engineering Mechanics, ASCE, 128(7), pp. 720-729, 2002. DOI: 10.1061/(ASCE)0733-9399(2002)128:7(720)
43. Park SS, Byrne PM (2004) Numerical modelling of soil liquefaction at slope site, fundamentals of soil dynamics, Proceedings of the International Conference on Cyclic Behavior of Soils and Liquefaction, pp. 571-580
44. Jefferies M, Been K (2006) Soil liquefaction - A critical state approach. Taylor & Francis, New York
45. Boulanger RW, Ziotopoulou K (2015) PM4Sand (Version 3): A sand plasticity model for earthquake engineering applications, Report No. UCD/CGM-15/01, Center for Geotechnical Modeling. University of California, Davis, CA, USA
46. Booker JR, Rahman MS, Seed HB (1976) GADFLEA - A computer program for the analysis of pore pressure generation and dissipation during cyclic or earthquake loading, Rep. No. EERC 76-24, Earthquake Engineering Research Center, Univ. of California at Berkeley, Berkeley, California, USA
47. Michael H, Beaty, Peter M, Byrne (2011) Documentation Report. UBCSAND Constitutive Model on Itasca UDM Web Site
48. Chou JC, Yang HT, Lin DG (2021) Calibration of Finn Model and UBCSAND Model for Simplified Liquefaction Analysis Procedures. Appl Sci 11:528
49. Ghalibafian H (2006) Evaluation of the effects of nonlinear soil-structure interaction on the inelastic seismic response of pile-supported bridge piers. University of British Columbia
50. Wood DM (2004) Geotechnical Modelling. CRC press
51. Hussein RS, Albusoda BS (2021b) Experimental Modelling of Single Pile under Combined Effect of Axially and Laterally Loadings in Liquefiable Soil. Geotechnical and Geological Engineering, 2021b. Accepted

52. Madhira RM, Jaswant NA (2000) Dilation of granular piles in mitigating liquefaction of sand deposits. Semantic Scholar, project of ground improvement
53. Chian SC, Madabhushi SP (2014) Soil Liquefaction–Induced Uplift of Underground Structures: Physical and Numerical Modeling. Geotech Geoenviron Eng, ASCE 140(10):04014057
54. Manish KA, Ashwani J, Nitish P (2017) Performance of pile foundations during Earthquake. ICET:EITM-2017-CE-529, Conference paper
55. Chian SC, Madabhushi SPG (2012) Effect of buried depth and diameter on uplift of underground structures in liquefied soils. Soil Dyn Earthq Eng 41:181–190
56. Mahmood Seid-Karbasi (2009) Effects of void redistribution on liquefaction-induced ground deformations in earthquakes: A numerical investigation. PhD Thesis, The university of British Columbia (Vancouver)

Figures

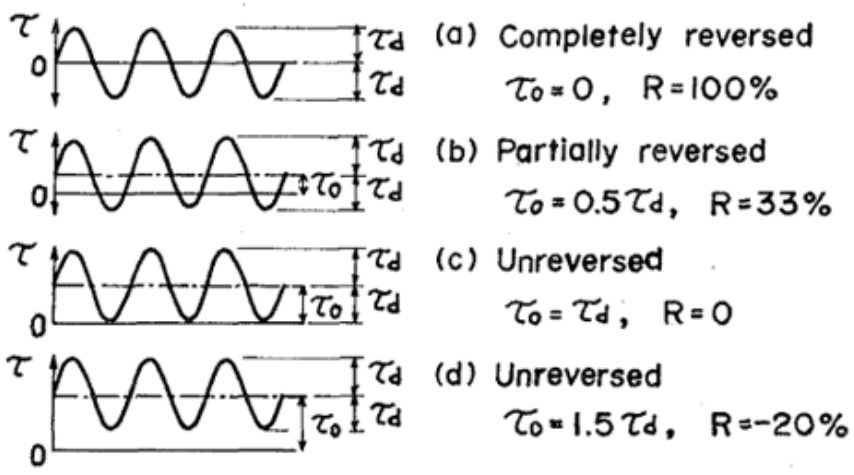

Figure 1

Stress reversal degree (Yoshiaki and Hrnosm, 1975).

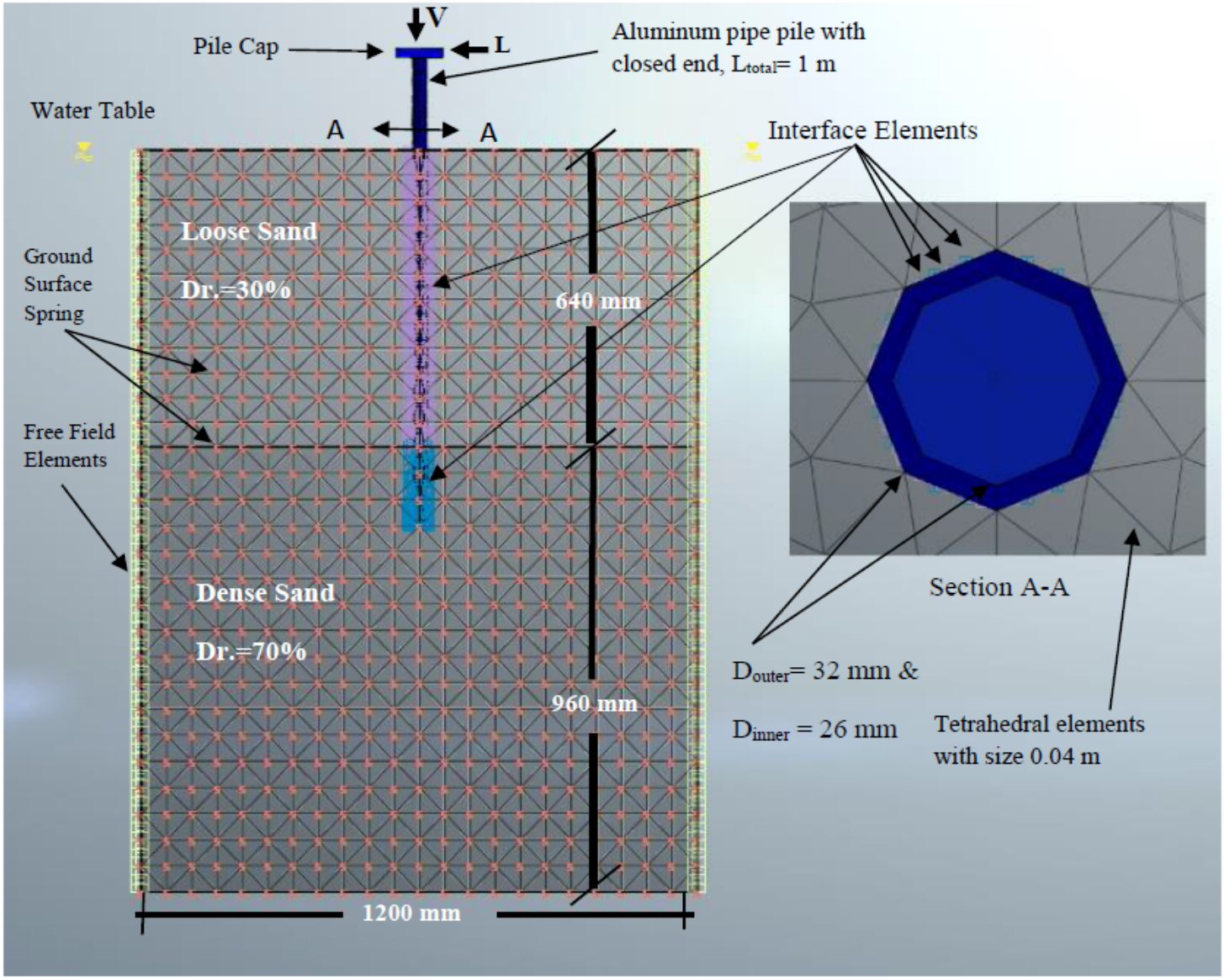

Figure 2

Longitudinal section of the geometry of the soil-pile model used in numerical Modelling-Scale η = 2.

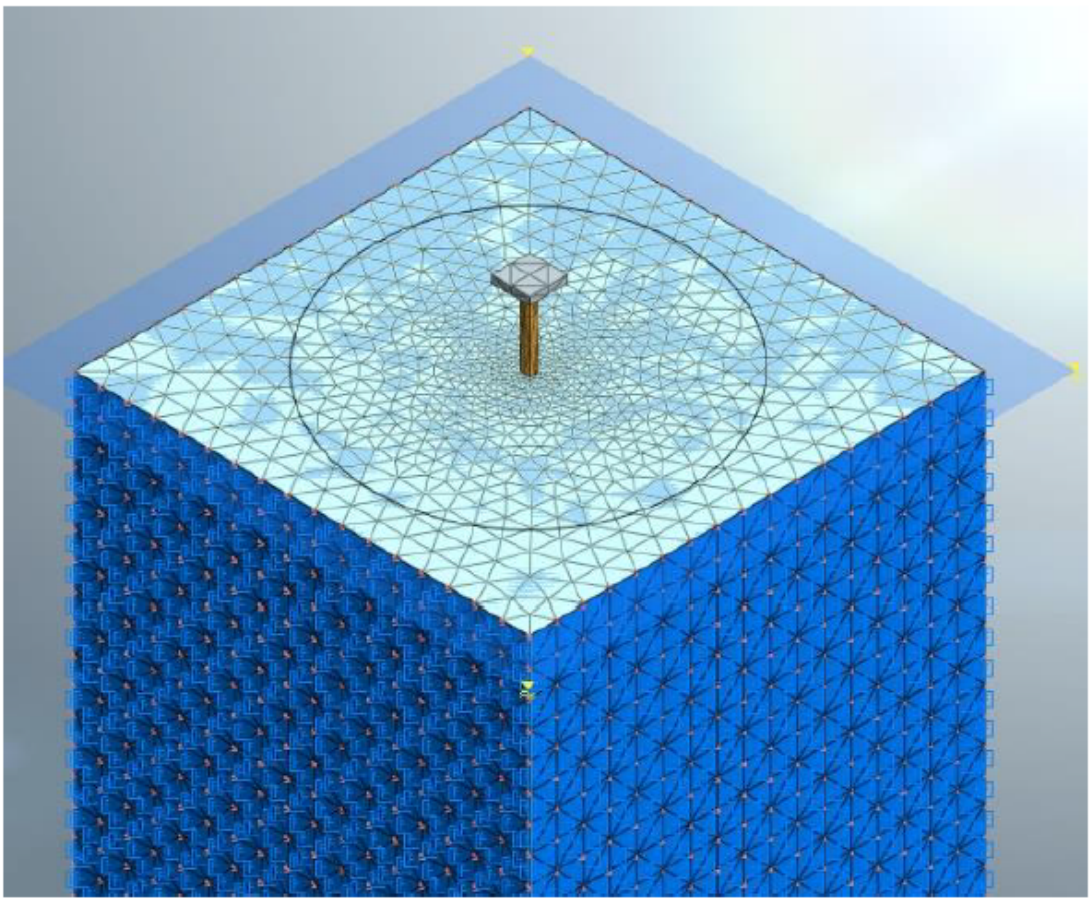

Figure 3

Mesh elements distribution.

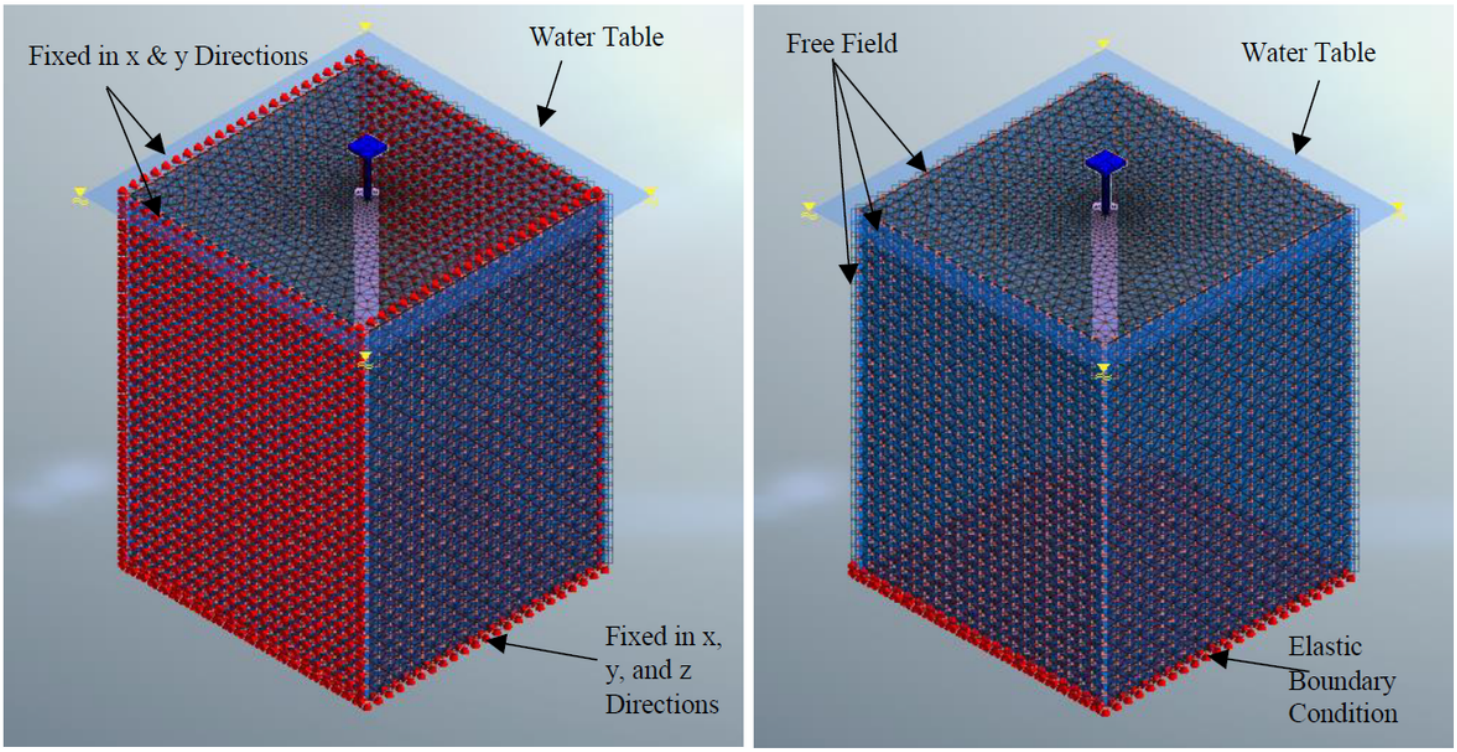

Figure 4

A full configuration of the model with its boundary condition for (a)static analysis, and (b) dynamic analysis

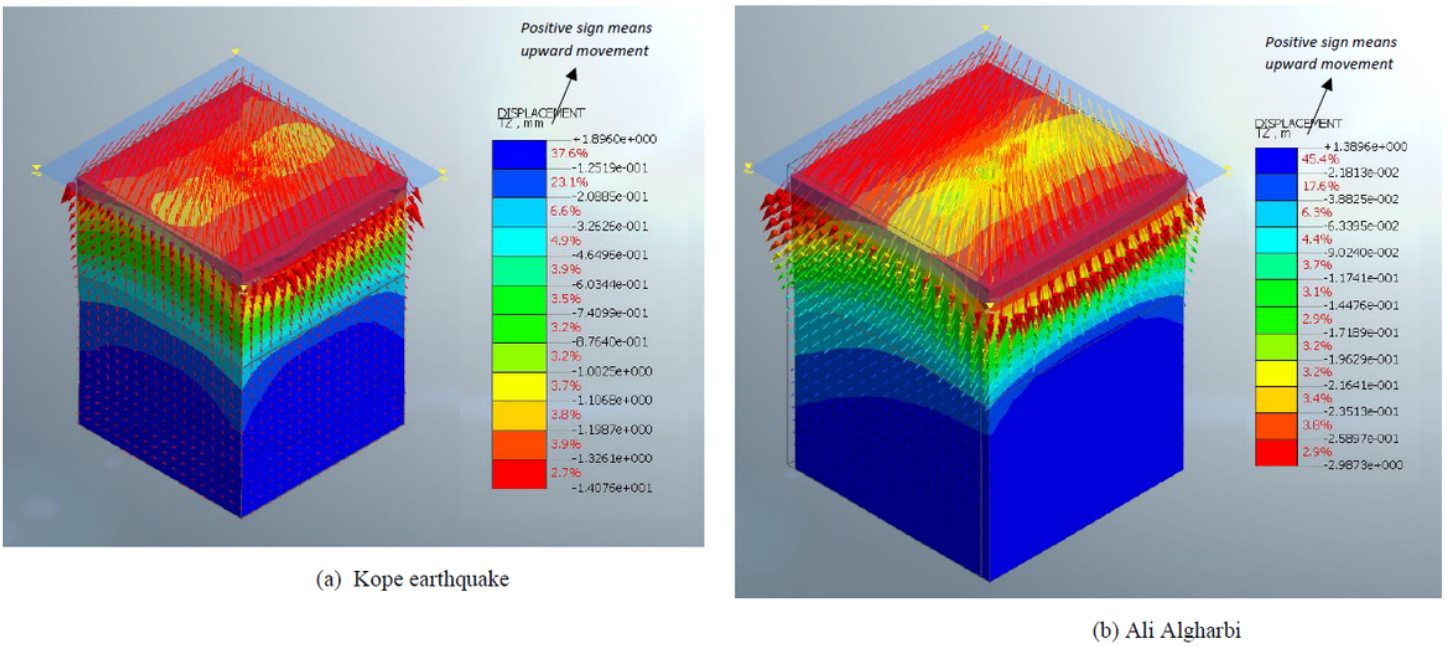

Figure 5

Maximum total deformation of soil layers (η = 2).

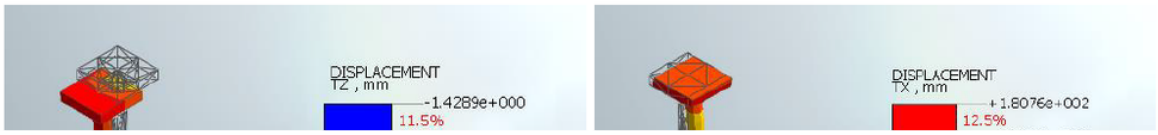

Figure 6

Maximum vertical and lateral displacement of the pile body (η = 2).

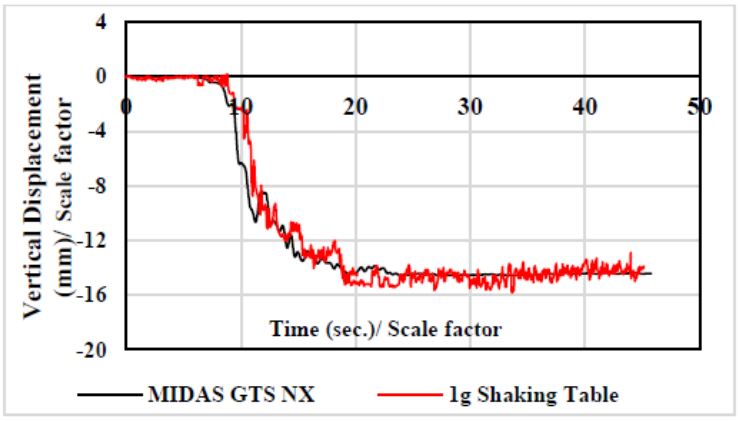

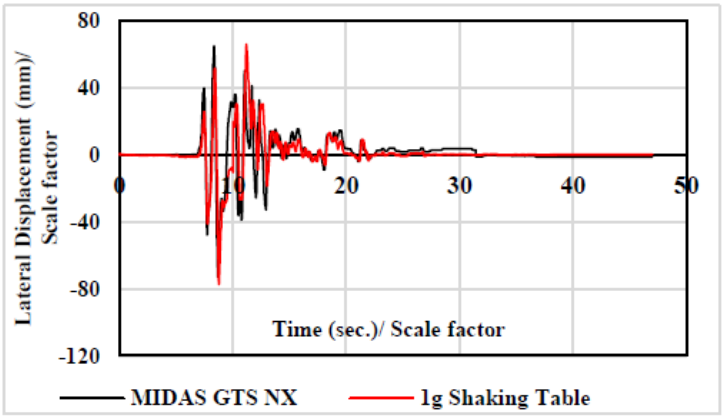

(a) Kope earthquake

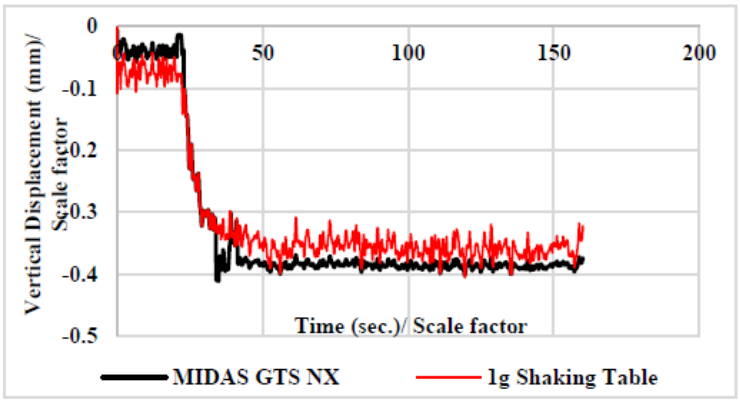

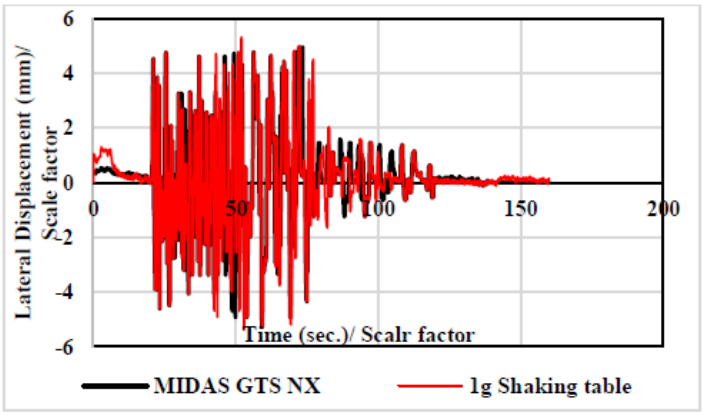

(b) Ali Algharbi earthquake.

Figure 7

Maximum deformation on the pile head during applying the coupled static and dynamic loads.

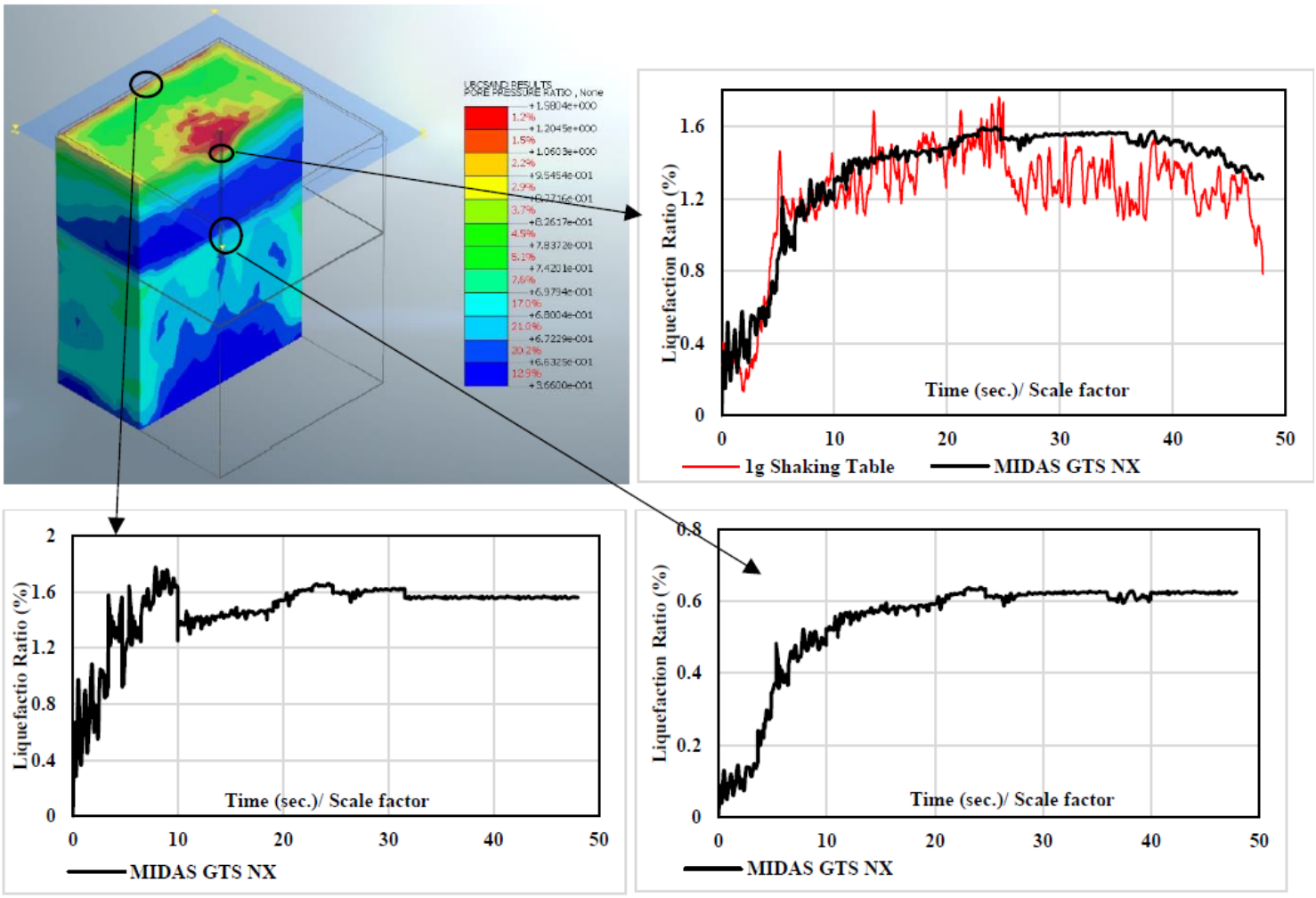

Figure 8

Maximum state of pore water pressure ratio (Kope earthquake).

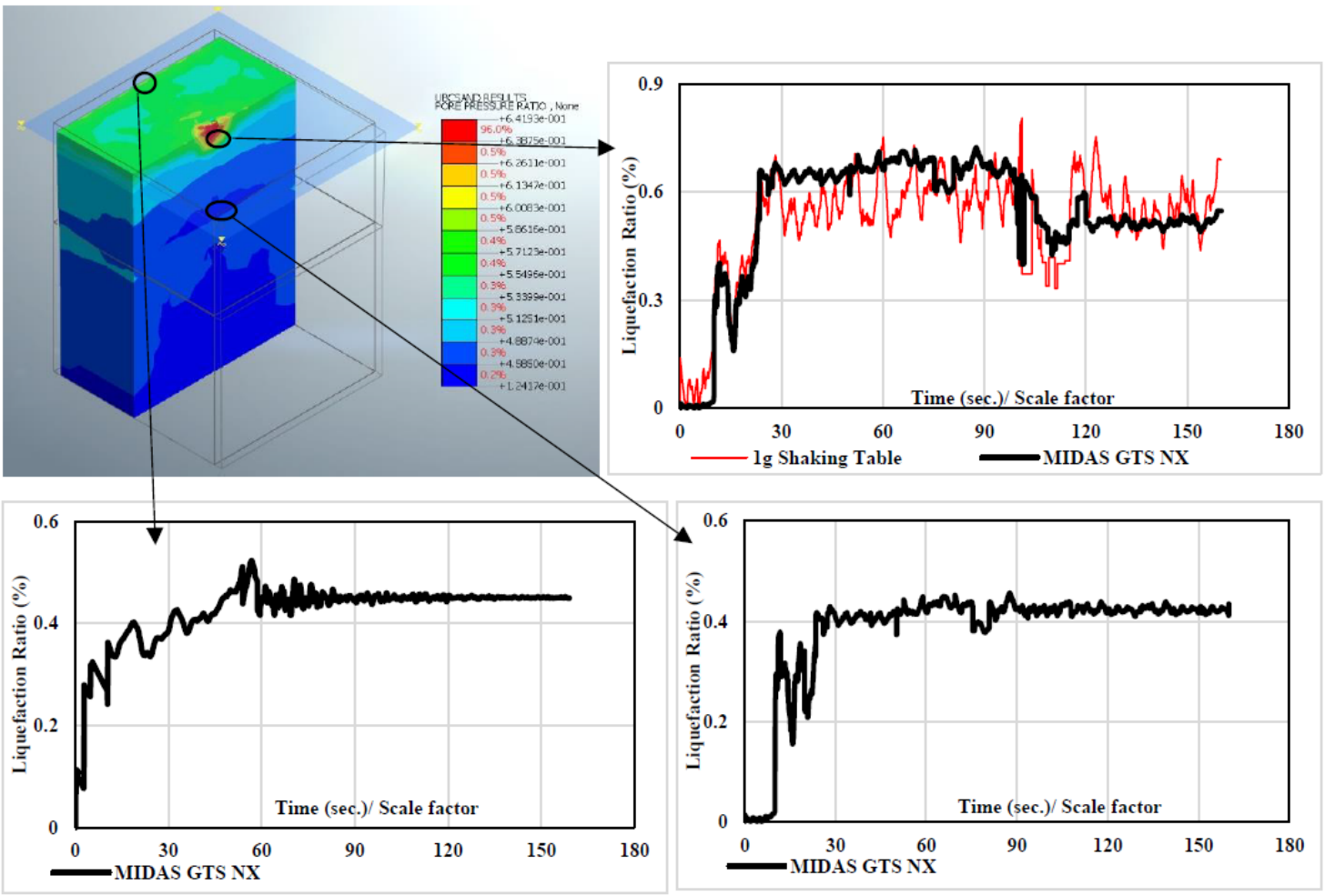

Figure 9

Maximum state of pore water pressure ratio (Ali Al-Agharbi).

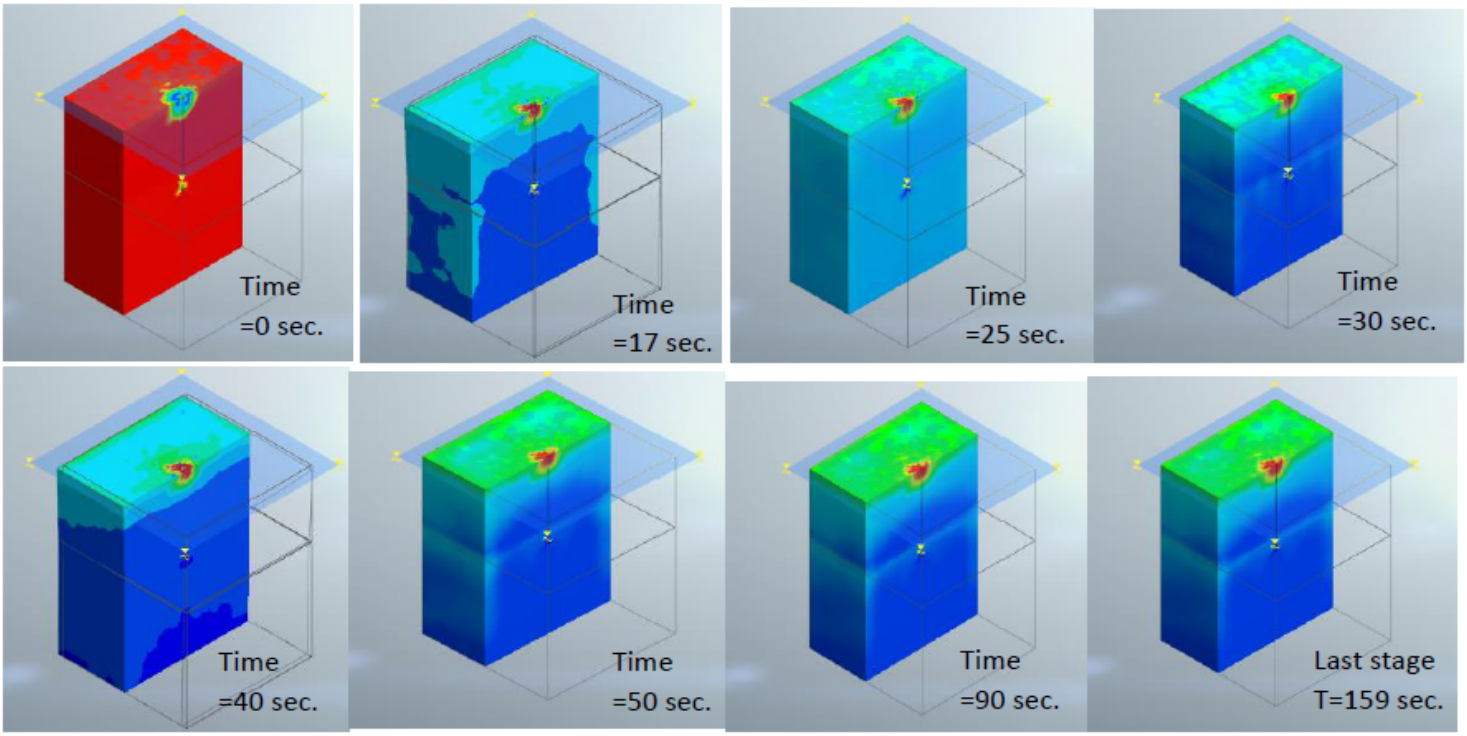

Figure 10

A pore water pressure distribution ratio of nonlinear time history analyses (Ali Algharbi).

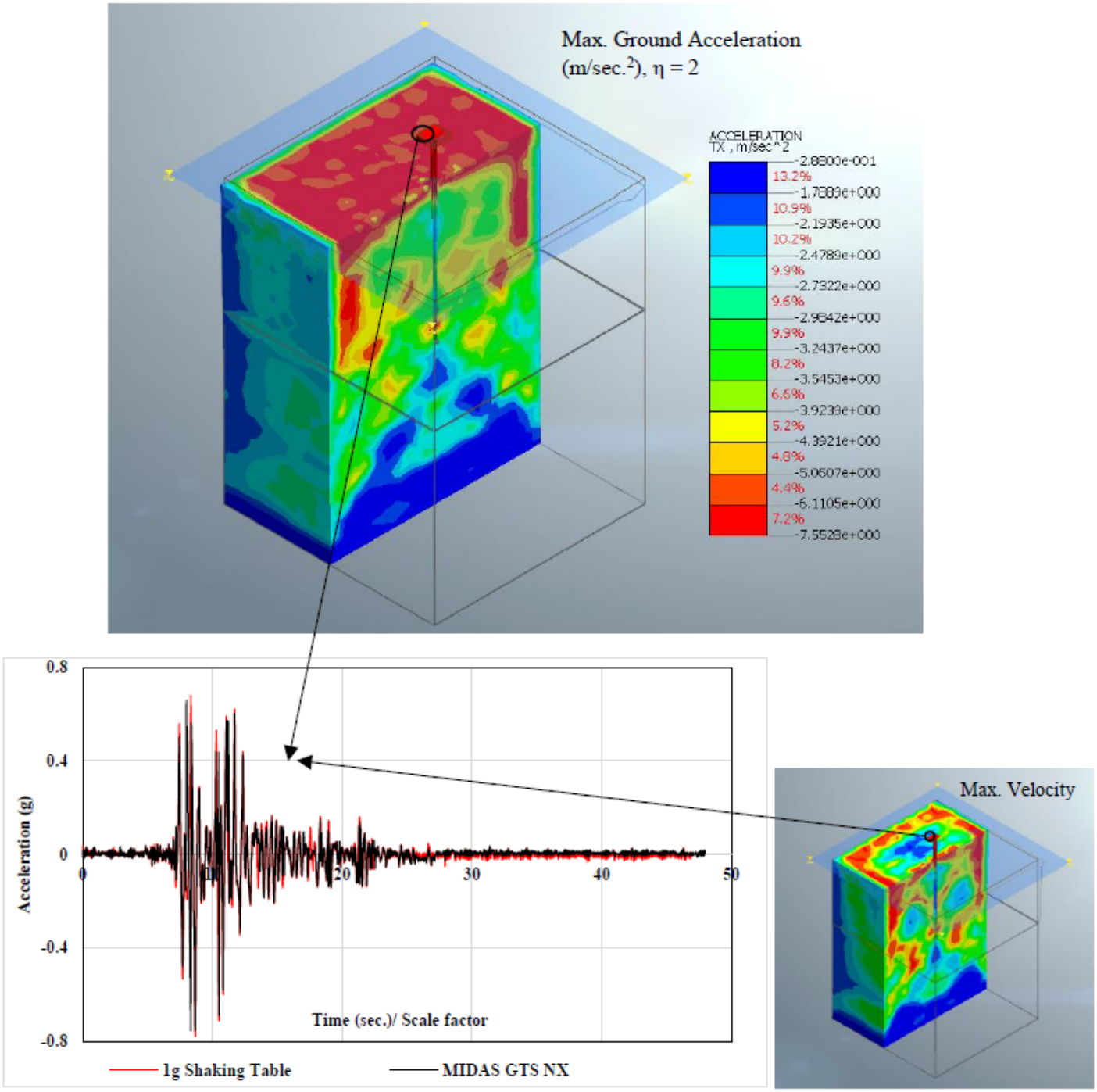

Figure 11

Acceleration time history (Kope earthquake).

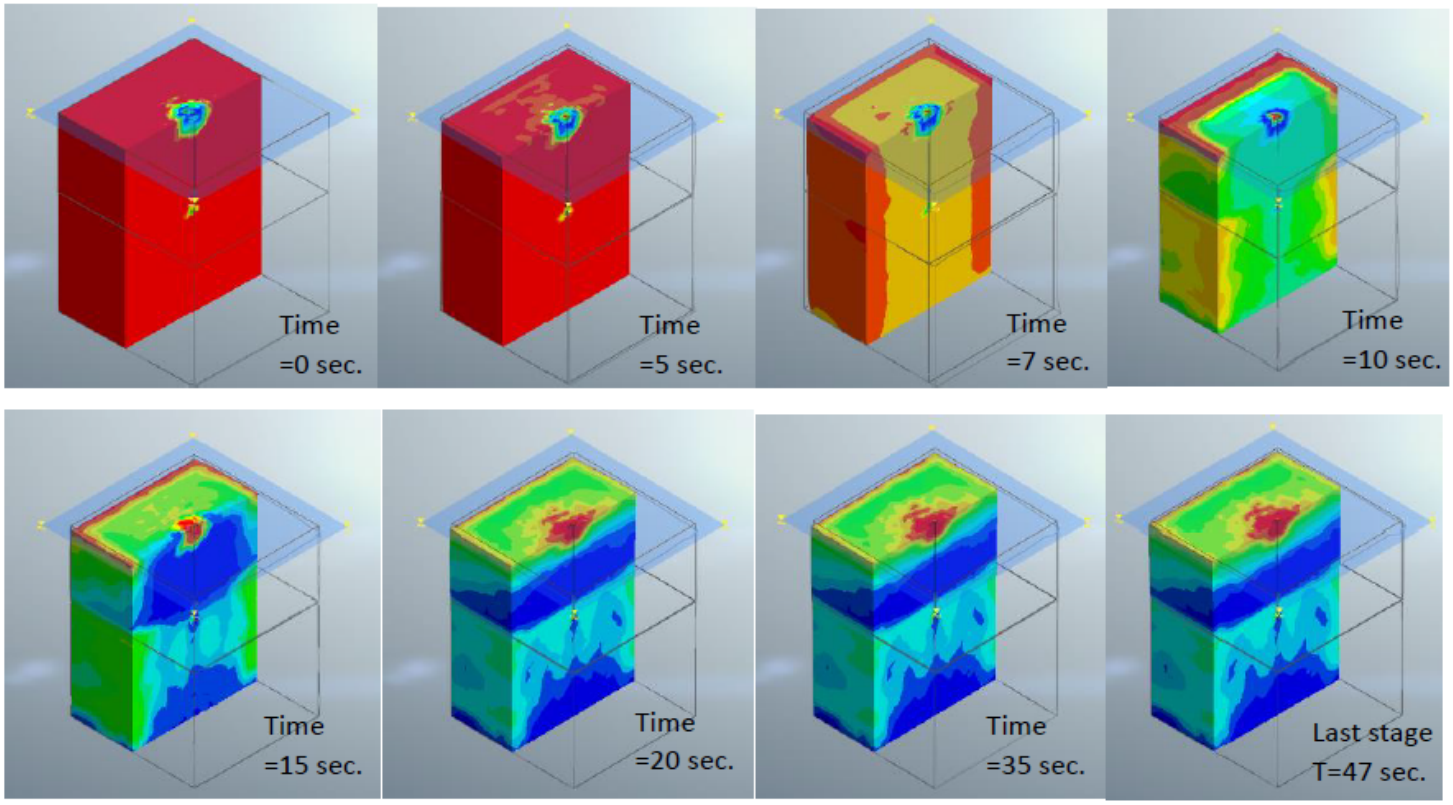

Figure 12

A pore water pressure distribution ratio of nonlinear time history analyses (Kope).

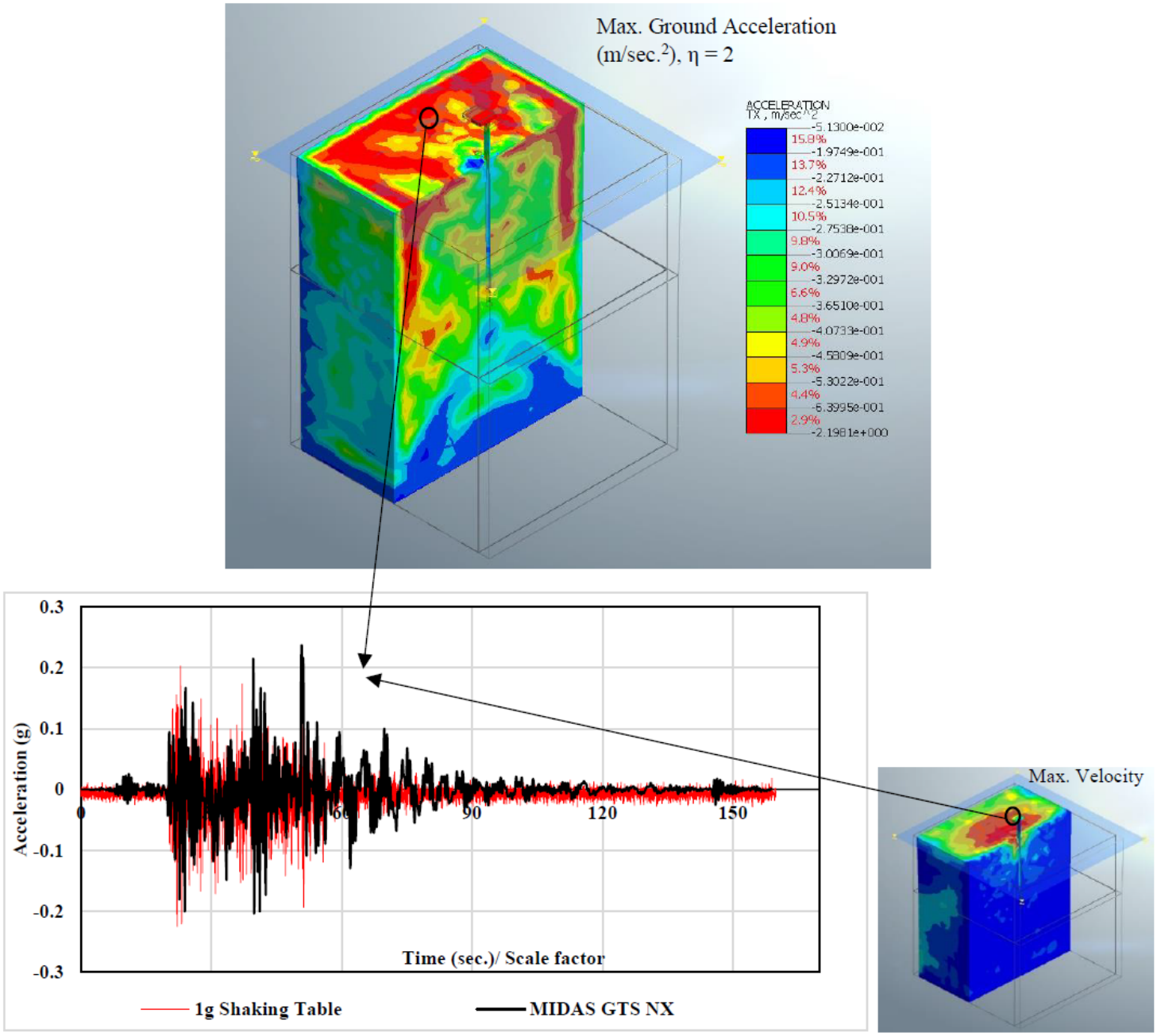

Figure 13

Acceleration time history (Ali Algharbi earthquake).

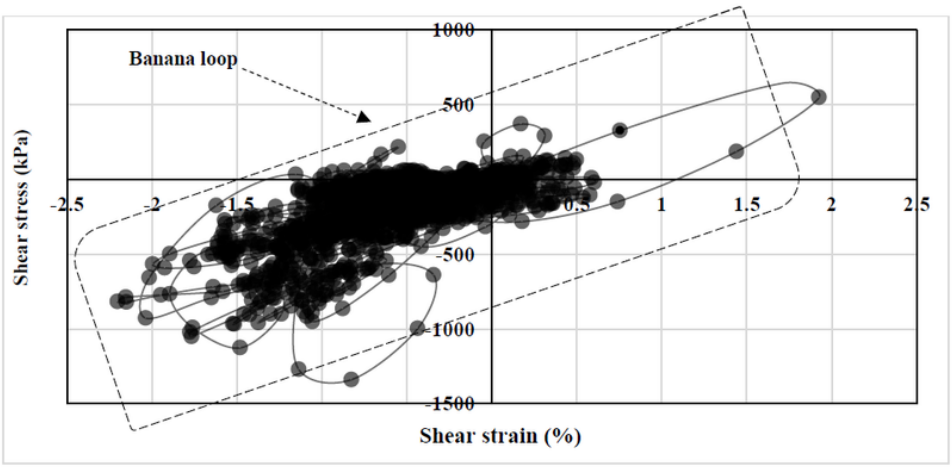

(a)

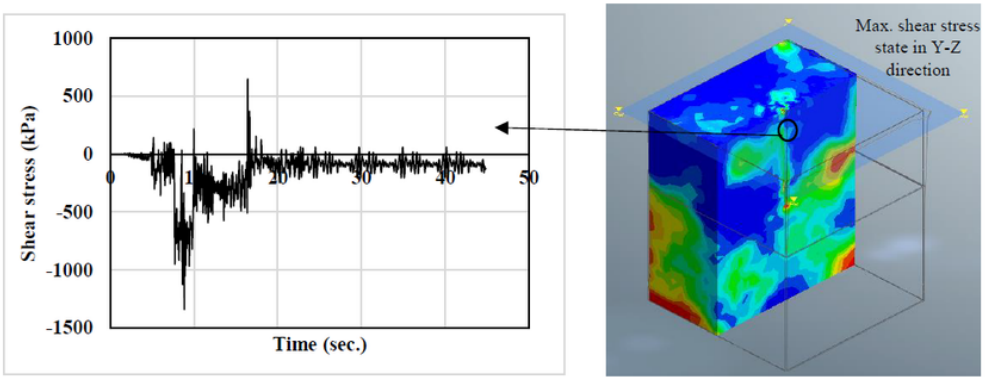

(b)

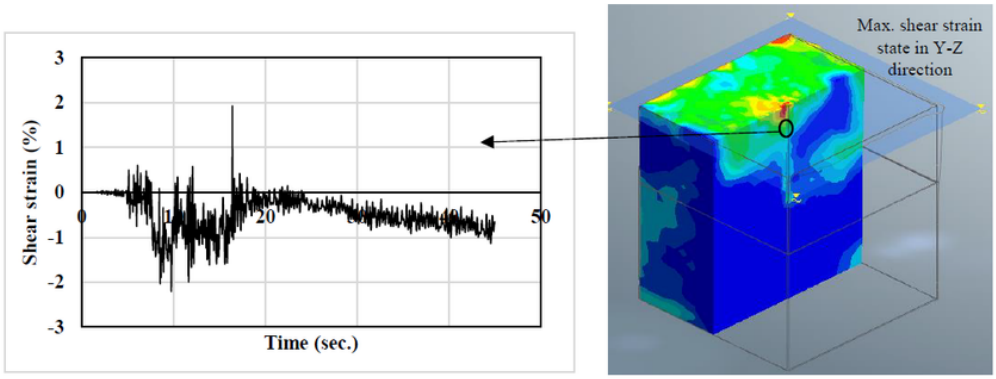

(c)

Figure 14

An undrained cyclic loading response of saturated sand soil under a coupled of static loads (vertical and lateral) and dynamic excitation (Kope earthquake).

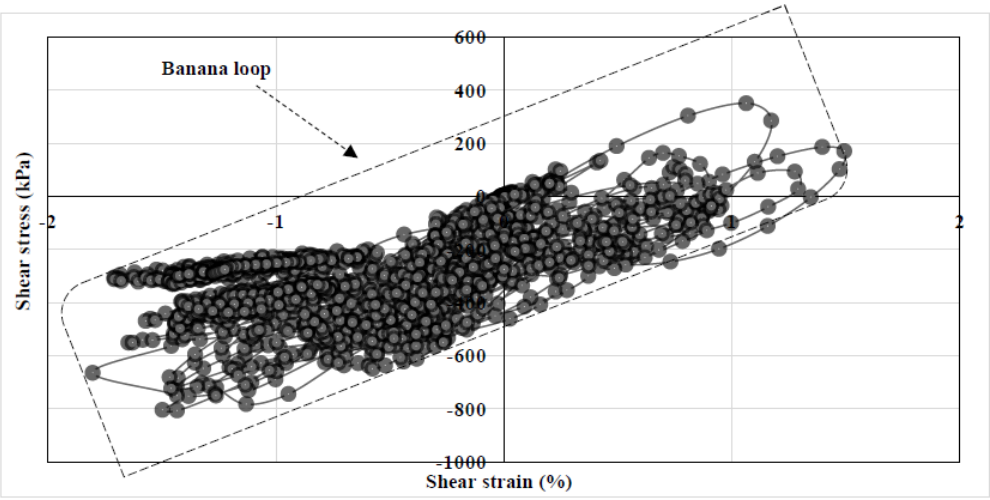

(a)

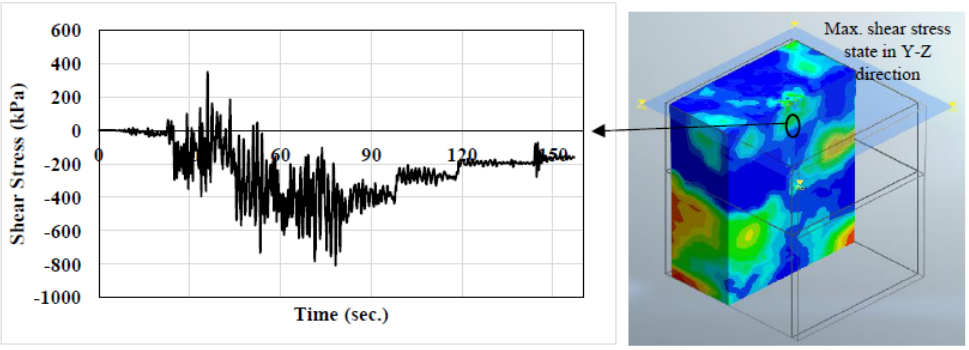

(b)

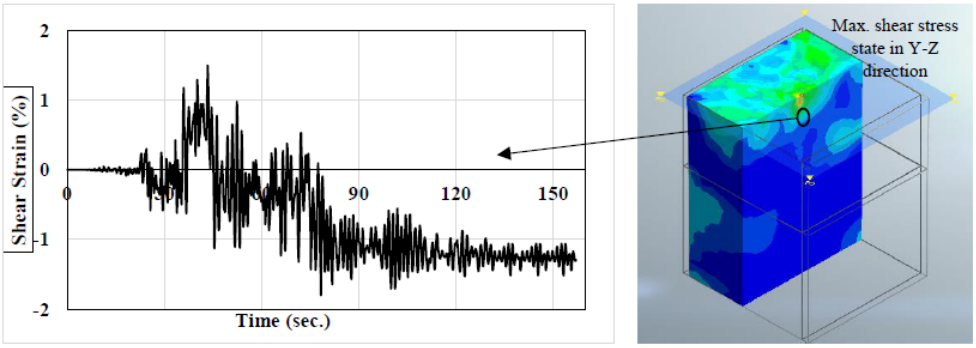

(c)

Figure 15

An undrained cyclic loading response of saturated sandy soil under a coupled of static loads (vertical and lateral) and dynamic excitation (Ali Algharbi earthquake).

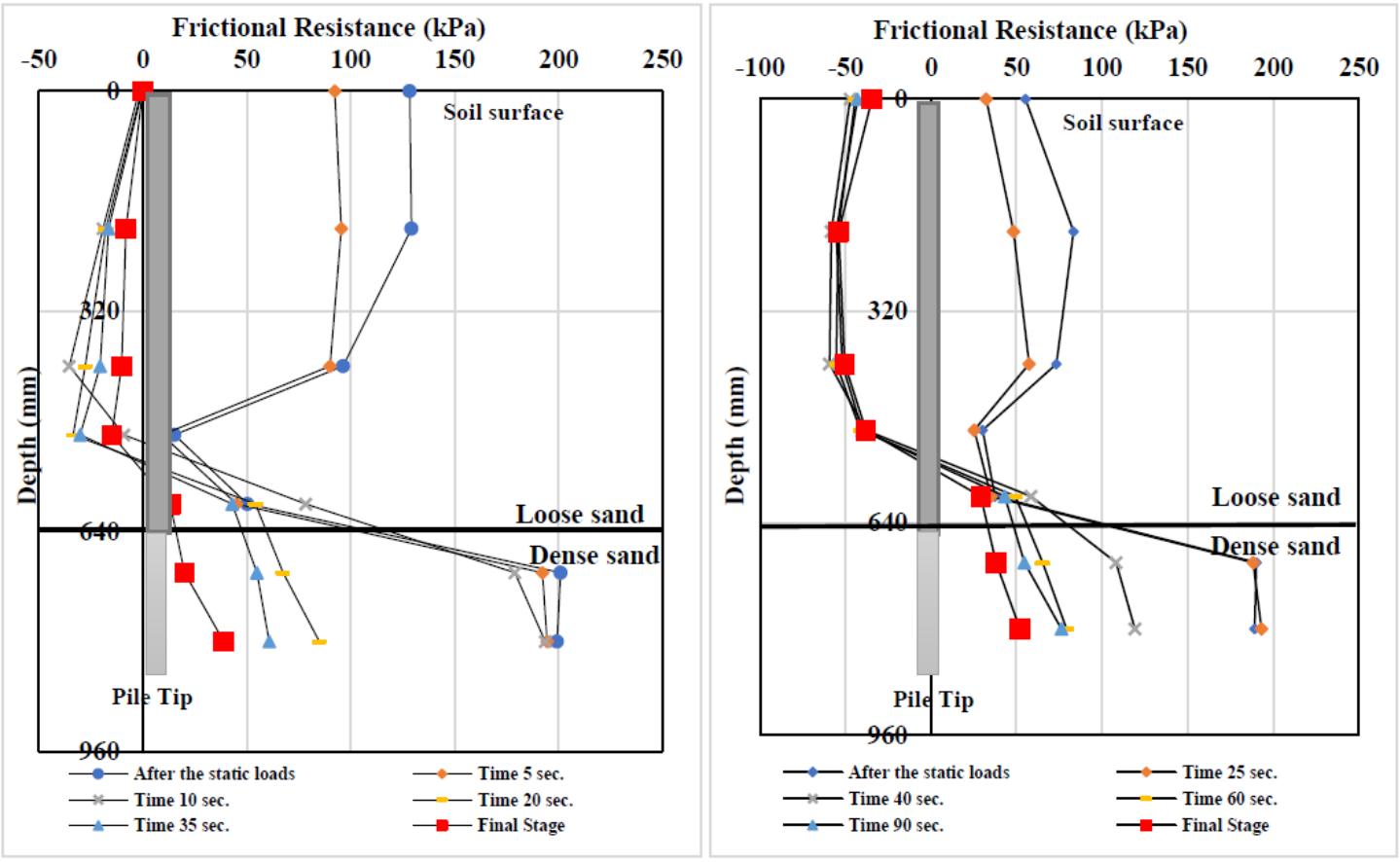

(a) Kope earthquake (b)Ali Algharbi

Figure 16

Numerical analyses of frictional resistance along the pile length embedded in saturated soil.